Stall delay and leading-edge suction for a pitching airfoil with trailing-edge flap

Guosheng He*, Julien Deparday†
UNFoLD, Institute of Mechanical Engineering, Federal Institute of Technology in Lausanne (EPFL), Switzerland

Lars Siegel ‡, Arne Henning§
German Aerospace Center (DLR), Institute for Aerodynamics and Flow Technology (AS), Göttingen, Germany.

and Karen Mulleners ¶
UNFoLD, Institute of Mechanical Engineering, Federal Institute of Technology in Lausanne (EPFL), Switzerland

The flow around a pitching NACA0015 airfoil with an oscillating trailing-edge flap is experimentally investigated to characterise the influence of the flap kinematics on the development of dynamic stall. We specifically focus on the timing of the stall development and critical values of the leading-edge suction parameter as a potential stall trigger. In general, static or dynamic trailing-edge flap motions strongly affect the entire lift response but preserve the characteristic evolution of the leading-edge suction parameter. The influence of the flap on the critical values of the leading-edge suction parameter and their timing is more subtle. Variations in the magnitude of the leading-edge suction are related to the instantaneous geometric effective angle of attack. A thin-airfoil theory based model that linearly superimposes the effect of the flap on the response for a fixed flap in its neutral position correctly predicts the maximum values of the leading-edge suction parameter. The timing at which these maxima are reached corresponds to the stall delay and is dominated by the pre-stall temporal evolution of the effective angle of attack. Our results suggest that dynamic stall development is governed by characteristic stall delays rather than critical values of the maximum leading-edge suction parameter.

I. Introduction

Dynamic stall refers to the phenomenon of unsteady separation occurring on airfoils undergoing time-varying motions. The dominant feature characterizing dynamic stall is the growth and shedding of a large-scale coherent dynamic stall vortex, after the airfoil angle of attack exceeds the static stall angle. The formation and convection of the dynamic stall vortex cause an overshoot of the lift, a delay in stall, and hysteresis of the lift history. Dynamic stall can lead to high aerodynamic loads or cause dangerous vibrations, which may result in a reduced performance or shortened

*Post-doctoral researcher, EPFL-STI-IGM-UNFoLD, Station 9, CH-1015 Lausanne, Switzerland.
†Post-doctoral researcher, EPFL-STI-IGM-UNFoLD, Station 9, CH-1015 Lausanne, Switzerland.
‡Doctoral candidate, DLR-AS-BOA, Bunsenstrasse 10, D-37073 Göttingen, Germany.
§Team leader Transport Systems, DLR-AS-BOA, Bunsenstrasse 10, D-37073 Göttingen, Germany.
¶Assistant professor, EPFL-STI-IGM-UNFoLD, Station 9, CH-1015 Lausanne, Switzerland. Senior Member AIAA.

life cycle of the structure. To protect the integrity and safety of the system, it is often desirable to mitigate or even eliminate the effects of dynamic stall. Popular methods to mitigate dynamic stall include boundary layer suction or blowing [1–3], applying plasma actuators [4–6],leading edge slats [7], deforming geometries [8], and trailing-edge flaps [9–11].

In potential flow theory, a deflection of the trailing-edge flap changes the camber of the airfoil, which changes the bound vorticity and the lift on the airfoil. If separation occurs either on the airfoil or on the flap, the flap no longer produces as much lift variation as predicted by the potential flow theory. However, that is not the case for a dynamic trailing-edge flap [12]. A dynamic trailing-edge flap can further increase the lift slope with respect to static measurements. After the flap motion stopped, the effectiveness would decrease to values consistent with steady-state measurements with separation. By taking into account the increased effectiveness of dynamic flaps, a better control of the unsteady lift can be achieved. Medina et al. [13, 14] investigated the influence of a 50 % flap that was rapidly deflected within a convective time scale. The front part of the wing in their study was fixed at 0° or 20°, which corresponds to attached and separated flow conditions. The transient lift responded immediately to the fast movement of the flap, regardless of initial flow conditions. For separated flows, a rapid flap deflection in both directions perturbed the leading edge shear layer dynamics and caused it to roll up into a leading edge vortex. The formation of this leading edge vortex explains the additional lift variations generated by a dynamic flap motion that are absent for a static flap deflection.

The dynamic lift response of a fixed airfoil with an active flap was systematically investigated by Pohl et al. [15] at a high Reynolds number of $Re = 1.8 \times 10^6$. The airfoil was fixed at 0° or 12° while different flap motion profiles are employed to obtain dynamic lift variations. The motion profiles included sinusoidal oscillations, ramp-up-ramp-down, and random sequences. For high flap actuation speeds during the sinusoidal and ramp motions, hysteresis emerges in the lift history. Flap separation was observed for high deflection angles above 10° and could be completely avoided if the residence time of the flap above this threshold angle was reduced, indicating the importance of understanding characteristic dynamic stall response and relaxation time scales.

Dynamic trailing-edge flaps have also been used to control dynamic stall. In most of these studies, a pulse-like actuation was used. The most important control parameters are the start time of the actuation with respect to the dynamic stall process, the actuation duration of the pulse, and the deflection amplitude of the flap. Gerontakos and Lee [16] tested the influence of all these parameters independently and quantified their influence on the dynamic stall lift and pitching moment and the wake flow structures. An early but longer flap actuation, in conjunction with an upward flap deflection would be more effective in reducing the nose-down pitching moment excursions. A parametric study of the flap actuation using discrete vortex method revealed that only upward flap deflections would lead to the reduction of aerodynamic damping [10]. The optimum actuation proposed would start between the mean and maximum airfoil angle of attack and last around one-third of the oscillation period. Active trailing-edge flaps also have the potential

to serve as primary flight control and vibration reduction devices and replace the conventional swash plate system in helicopters [17].

The studies on pulse-like flap actuation are important in understanding the transient response of the loads on the airfoil and have demonstrated their effectiveness to mitigate gusts. But some disturbances in practice are continuous in nature. The dynamic stall control adopting continuous flap motion is not as extensively studied in the literature. Krzysiak and Narkiewicz [18] measured the unsteady aerodynamic loads on a pitching airfoil with a trailing-edge flap deflecting twice as fast as the main airfoil. The influence of phase delay between airfoil pitching and flap deflection was considered. The higher harmonic oscillations of the flap lead to dual loops of the lift and moment polars. A phase shift between the airfoil and flap oscillation has a significant influence on the lift and pitching moment coefficients. When the angle of attack of the airfoil and flap deflection increase simultaneously, there is an increase of maximum lift coefficient, and when the two angles decrease simultaneously maximum lift coefficient decreases. Lee and Su [19] investigated the effects of a trailing-edge flap that is actuated at different start times and amplitudes. Here, a delayed start of the flap motion was compensated by a faster flap deflection compared to the pitch rate of the oscillating airfoil to keep the oscillation periods the same for both components. Large changes in the dynamic load hysteresis loops were observed but the formation and detachment of the dynamic stall vortex were largely unaffected by the flap deflection, regardless of the starting time of the flap actuation. The effectiveness of the trailing-edge flap control scheme was comparable to that obtained via a pulsed ramp flap motion.

An accurate way to predict the onset and growth of the dynamic stall vortex is essential for successful modeling of the dynamic stall process and the effectiveness of a trailing-edge flap. The leading edge suction parameter was proposed as a criterion for the discrete vortex shedding from the leading edge [20, 21]. For any airfoil and Reynolds number, they suggested the existence of a maximum allowed leading edge suction or critical value of the leading edge suction parameter, which is independent of the motion kinematics. A vortex will shed from the leading edge when the instantaneous leading edge suction parameter exceeds that critical value. This augmented discrete vortex method using just a single empirical parameter, the critical leading edge suction parameter value, is an elegant approach to predict the onset, growth, and termination of the leading edge vortex and the unsteady aerodynamic responses for different airfoils and motion kinematics [22–25].

Past efforts have shown the potential to considerably affect the dynamic stall response of an airfoil by using a dynamic trailing edge flap. In this study, we want to further explore the concept of a critical leading edge suction parameter as a potential stall trigger or indicator for a range of dynamic stall scenarios created by a dynamic trailing-edge flap. We experimentally study the effect of a harmonically oscillating trailing edge flap on a NACA0015 airfoil using time-resolved velocity field and surface pressure measurements. Our focus is on characterizing the influence of different phase shifts between the main airfoil and the flap oscillations on the evolution of the leading edge suction parameter and the dynamic stall delay.

II. Experimental setup

The experiment was conducted in a recirculating wind tunnel at the German aerospace center in Göttingen. The open jet test section of the tunnel has a nozzle end size of 0.75 m × 1.05 m. The tunnel was operated at an incoming free stream velocity of U_∞ = 30 m/s. A NACA0015 airfoil was placed horizontally in the center of the test section. The span of the airfoil was 1.05 m and the chord length c = 0.3 m. The Reynolds number based on the chord length is $Re = 5.5 \times 10^5$.

A sketch of airfoil and the pitching mechanism is shown in figure 1. The airfoil was pitched around the quarter chord axis (0.25 c) and has a movable trailing-edge flap with the rotation axis at 0.7 c. Both the airfoil and the flap were 3D printed and the surface was painted black to keep it smooth and to reduce the reflection of the laser light. The gap at the flap hinge between the main airfoil and the flap was covered with flexible tape to ensure a smooth transition on the surface. Preliminary tests with and without the tape revealed negligible influence of the tape and the gap. The main airfoil was connected to a Nanotec DB87L01 Brushless DC motor using a stainless steel shaft. This motor, equipped with a planetary 25:1 gear, gives a rated torque output of 52.5 N m. The flap was connected to a second brushless DC motor (Nanotec DB43C048030) using an aluminium alloy shaft. This flap motor is equipped with a planetary 20:1 gear and gives a rated torque output of 8.8 N m. The flap motor and support were attached and fixed to the main airfoil shaft and move together with the main airfoil (figure 1a). The motion of the two motors were synchronized and individually controlled by a Galil DMC-4040 motion controller. The main airfoil was pitched around its static stall angle $\alpha_0 = \alpha_{ss} = 20°$ with an amplitude of $\alpha_1 = 8°$ and frequency of f_{osc}. The reduced frequency $k = \pi f_{osc} c/U_\infty$ for the main airfoil for the presented data is 0.1. The flap is either fixed at angle $\beta \in \{-20°, -10°, 0°, 10°, 20°\}$ or oscillated around its neutral position $\beta_0 = 0°$ with an amplitude of $\beta_1 = 20°$. The oscillation frequency of the flap equals the frequency of the main airfoil. The phase lag $\Delta\Phi$ between the trailing-edge flap and main airfoil oscillation is varied from $-\pi$ to π.

The unsteady airfoil surface pressure distribution is measured in the mid-span section of the airfoil. A total of 36 differential pressure transducers (Endevco model 8510B-1) are buried inside the wing and connected to the surface pressure holes using plastic tubes with a 1 mm inner diameter and a length of less than 200 mm. The pressure transducers have a measurement range of 0 kPa to 6.89 kPa and a resonance frequency of 55 kHz. We have 20 pressure holes on the suction side and 16 along the pressure side (figure 1b). The sampling rate for pressure measurements is 20 kHz. Surface pressure data is recorded for 78 pitching cycles. The lift response is obtained by integrating the pressure distribution around the airfoil. The pressure data from the first 10 % of the chord was used to calculate the leading edge suction parameter using the procedure described by [25]. The leading edge suction vector S_{LE} is calculated by integrating the pressure force based on the 13 pressure sensors in the front 10 % of the airfoil. The magnitude of the leading edge suction vector is indicated by $|S_{LE}|$ and its angle with respect to the incoming flow by λ. The experimental leading edge

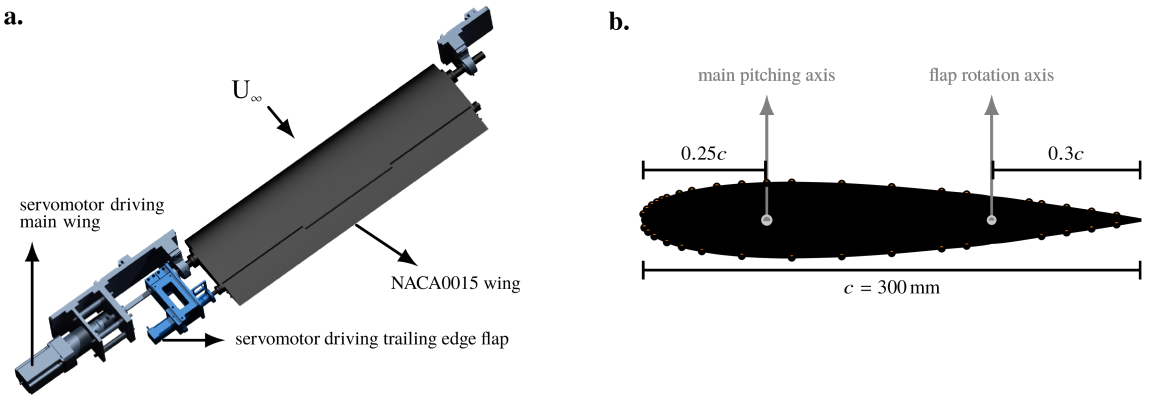

Figure 1 (a) Pitching mechanism for the main airfoil and the trailing edge flap, (b) positions of the pitching axes and the pressure transducers.

suction parameter is the projection of the leading edge suction vector onto the chordwise direction:

$$A_{0,\mathrm{exp}} = \mathrm{sign}(S_{\mathrm{LE}})\sqrt{\frac{2}{\pi}|S_{\mathrm{LE}}|\cos(\lambda-\alpha)} \quad . \tag{1}$$

where α is the instantaneous angle of attack of the airfoil and $\mathrm{sign}(S_{\mathrm{LE}})$ is negative when the suction vector is pointing downstream and positive when pointing upstream.

Two-dimensional particle image velocimetry (PIV) is used to measure the flow field at the mid-span of the airfoil. The flow field is illuminated by a dual-pulsed Quantronix laser and the particle images are recorded by a PCO DIMAX HS camera with a 1800 px × 1600 px sensor. The camera is zoomed in around the leading edge and the field of view covers the front 20 % of the airfoil. The sampling rate for the PIV is 1.5 kHz. A multi-grid algorithm was used to obtain the velocity vectors with the final window size of 48 px × 48 px and 50 % overlap yielding a physical grid resolution of 1.83 mm = 0.0061 c in the leading edge region.

III. Results

When a trailing edge flap is deflected, it changes the effective angle of attack and camber of the airfoil (figure 2). The effective angle of attack is defined as

$$\alpha_{\mathrm{eff}} = \alpha + \Delta\alpha = \alpha + \arctan\left(\frac{0.3\sin\beta}{0.7+0.3\cos\beta}\right) \tag{2}$$

for a flap with length of 0.3 c. Here, α indicates the angle of attack of the main wing and β is the flap angle deflection. We only take into account the purely geometric effect of the flap deflection and not its influence on the leading edge stagnation point nor the induced effects resulting from an unsteady pitch or flap angle variation. The flap angle β is defined positive when it is deflected downward and increases the effective angle of attack and leads to a positive

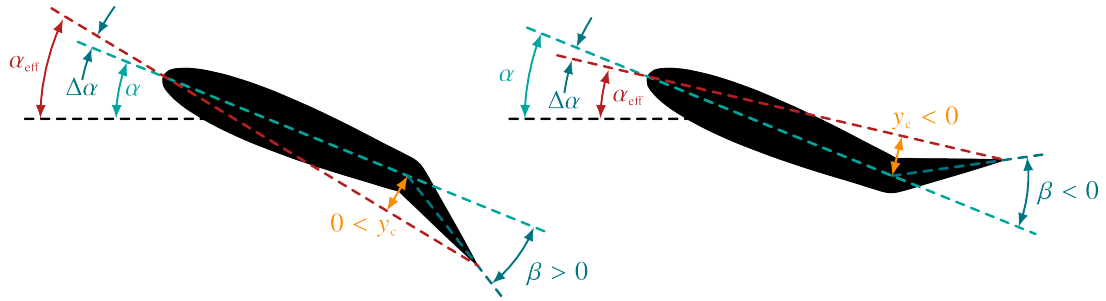

Figure 2 Definition of the geometric effective angle of attack and camber as a result of the trailing edge flap defection.

camber y_c. When the flap angle is negative, the effective angle is smaller than the angle of attack of the main wing and the airfoil has negative camber (figure 2). The maximum camber is always located at the flap hinge and increases with flap angle according to

$$y_c = 0.7c \sin \Delta\alpha \quad . \tag{3}$$

For the maximum flap deflection of 20° which we consider here, we find maximum values of $\Delta\alpha = 6°$ and $y_c = 0.07c$.

A. Static lift and leading edge suction response

The static lift responses for fixed trailing edge flap angles $\beta \in \{-20°, -10°, 0°, 10°, 20°\}$ are presented in figure 3a. The error bars represent the standard deviations of the signals at the static angles of attack and do refer to a measurement error but are a measure for the inherent fluctuations of the pressure signals due to flow unsteadiness. Without flap deflection, the airfoil is symmetric and generates zero lift at zero angle of attack, has a lift slope of 0.87π prior to stall and a static stall angle of 20°. The lift slope is much lower than the theoretical value of 2π and the stall angle is higher than expected from numerical simulation or measurements in closed test sections facilities because our experiments have been conducted in a wind tunnel with an open test section. Wind tunnel corrections for open jet flows by Ewald [26] allow to compensate for the observed variation in the lift slope but are only applicable to fully attached flows and have not been applied to the presented data.

For positive flap angles, the effective camber increases and the static lift polar is shifted up along the lift axis. For negative flap angles, the effective camber decreases and the static lift polar is shifted down along the lift axis. The lift slopes prior to stall remain approximately the same for all flap angles and the static stall angle based on the maximum lift peak varies only slightly from 20.5° to 19° between the largest negative and largest positive flap angle. The trailing edge flap deflection substantially alters the lift generated but does not seem to have a major influence on the critical conditions that lead to stall.

In recent years, the leading edge suction parameter has received renewed attention as a potential indicator and critical stall parameter [22–24]. In our previous work [25], we showed the increase of the critical leading edge suction

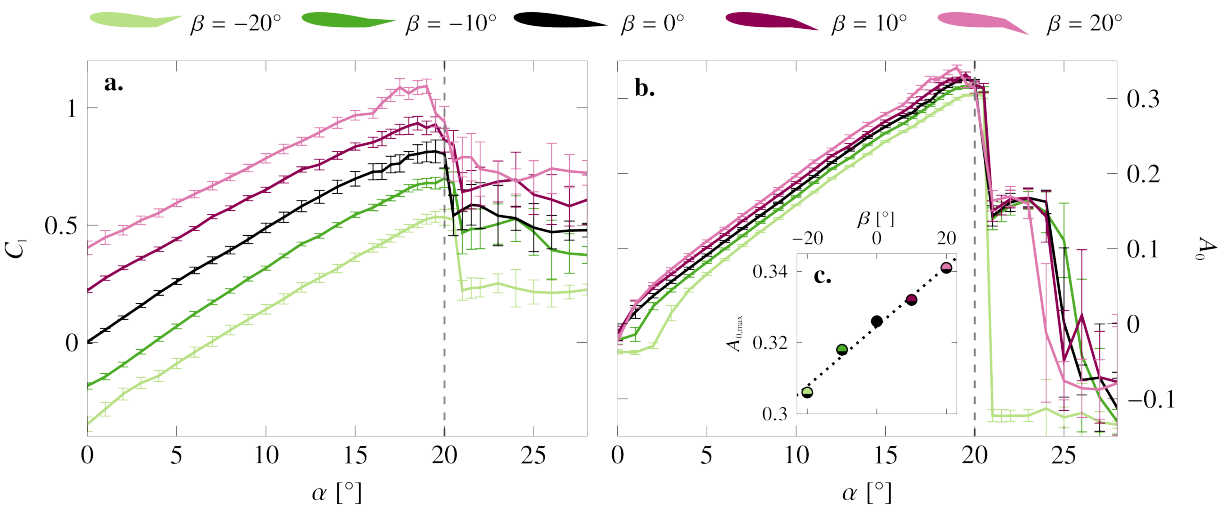

Figure 3 (a) Static response of the lift coefficient C_l and (b) leading edge suction parameter A_0 as a function of the geometric angle of attack of the main wing α for fixed deflections of the trailing edge flap $\beta \in \{-20°, -10°, 0°, 10°, 20°\}$. The inset (c) shows the variation of the maximum leading edge suction parameter with flap deflection angle.

parameter with increasing unsteadiness of the pitching motion. Here, we want to build upon these efforts and further explore the influence of a trailing edge flap deflection and motion on the critical leading edge suction.

The static response of the leading edge suction parameter A_0 as a function of the main wing angle of attack is presented in figure 3b. The leading edge suction increases approximately linearly with angle of attack when the flow is attached. The rate of increase of the leading edge suction is the same for all flap deflection angles and curves have a clear drop off between $\alpha = 20°$ and $\alpha = 21°$. The maximum value that the leading edge suction parameter reaches, increases linearly with increasing flap deflection angle (figure 3c). This maximum value is a measure for the maximum leading edge adverse pressure gradient that the airfoil can sustain before stalling [20, 27, 28]. The influence of the flap defection on the static response of the leading edge suction is considerably smaller than the influence on the lift coefficient. This suggests that the main difference in lift is not generated near the leading edge but distributed over the entire chord. As a consequence, the leading edge adverse pressure gradient is only slightly affected and the critical leading edge values and stall angles vary no more than 10 % or 1° for flap deflections angles from β =−20° to 20°. But the small variations we detect are consistent and indicate that a higher flap angle leads to a higher critical leading edge suction value and a lower static stall angle.

B. Dynamic lift response for an oscillating trailing-edge flap

The dynamic lift responses for a sinusoidally oscillating airfoil with oscillating trailing edge flap are summarised in figure 4. The temporal evolution of the effective angle of attack and phase averaged lift coefficient are presented in figure 4a-b for different phase delays $\Delta\phi$ between the main wing and the flap oscillation indicated by the colour of the

curves. The bottom x-axis shows the convective time with respect to the time at which the static stall angle of 20° has been exceeded. The top axes indicate the geometric angle of attack of the main wing and the time normalised by the pitching period. The main wing and the flap oscillate with the same frequency and the pitching period starts at when the main wing is at the minimum angle of attack. The dashed line represents the lift evolution for the airfoil with the flap fixed at 0°. The effective angle of attack is calculated according to equation (2). Negative phase delays correspond to motions where the flap motion leads the main wing motion such that the maximum effective angle is reached in the first half of the cycle. Positive phase delays correspond to motions where the flap motion lags the main wing motion such that the maximum effective angle is reached in the second half of the cycle. The motions are in-phase when the main wing angle α and the flap angle β increase and decrease together such that they reach the highest possible effective angle of attack in the middle of the pitching cycle. The maximum and minimum values of the effective angle respectively decrease and increase with increasing phase shift leading to a decrease of the effective pitch angle of attack amplitude with increasing absolute value of the phase delay (figure 4c). The time averaged mean effective angle remains at 20° for all motions, which corresponds to the static stall angle of attack α_{ss}. The effective angles of attack that are reached when the main wing angle exceeds the static stall angle are higher than 20° if the flap is leading the main wing and lower than 20° when the flap is lagging the main wing and equal to 20° when the flap and main wing are in or 180° out-of-phase (figure 4c).

The dynamic stall lift responses for the oscillating trailing-edge flap vary widely with the phase delay between the flap and the main wing. In general, the lift coefficient is higher in the first part of the cycles when the flow is attached and decreases during the second part of the cycle where increased values of the standard deviation, represented by the error bars, indicate flow separation. The error bars do not indicate experimental uncertainly or error here, but are a measure for the inherent fluctuations of the pressure signals due to the unsteadiness of the flow and cycle-to-cycle variations [29, 30]. In most cases there are two peaks in the high angle of attack range ($24° < \alpha < 28°$). The first peak indicates the main dynamic stall lift overshoot that is reached when the shear layer starts to roll up into the primary dynamic stall vortex. The second peak is associated with the additional vortex lift due to the presence of the dynamic stall vortex on the airfoil. The time average lift coefficient lies within $\bar{C}_{l,noflap} \pm 0.04$ with $\bar{C}_{l,noflap}$ the time averaged lift coefficient for the pitching motion with fixed flap at 0° indicated by the dashed line in (figure 4b). The time averaged lift values of the leading flap motions are slightly above the no-flap value and the values of the lagging motions are slightly below. The vertical lines in figure 4d indicated the range of C_l-values spanned by the phase averaged dynamic stall curves. The range of lift values spanned by the motion with fixed flap at 0° are indicated by the dotted lines. The effective angle of attack amplitude decreases with increasing absolute value of the phase delay leading to smaller fluctuations of the lift coefficient. The lift excursions for the motion with the flap leading by $\pi/4$ are highest even though this motion covers the same effective angle of attack range as the motion with the flap lagging by $\pi/4$. The effective angles of attack during the first half of the cycle and thus pre-stall are higher for motions where the flap leads. This leads

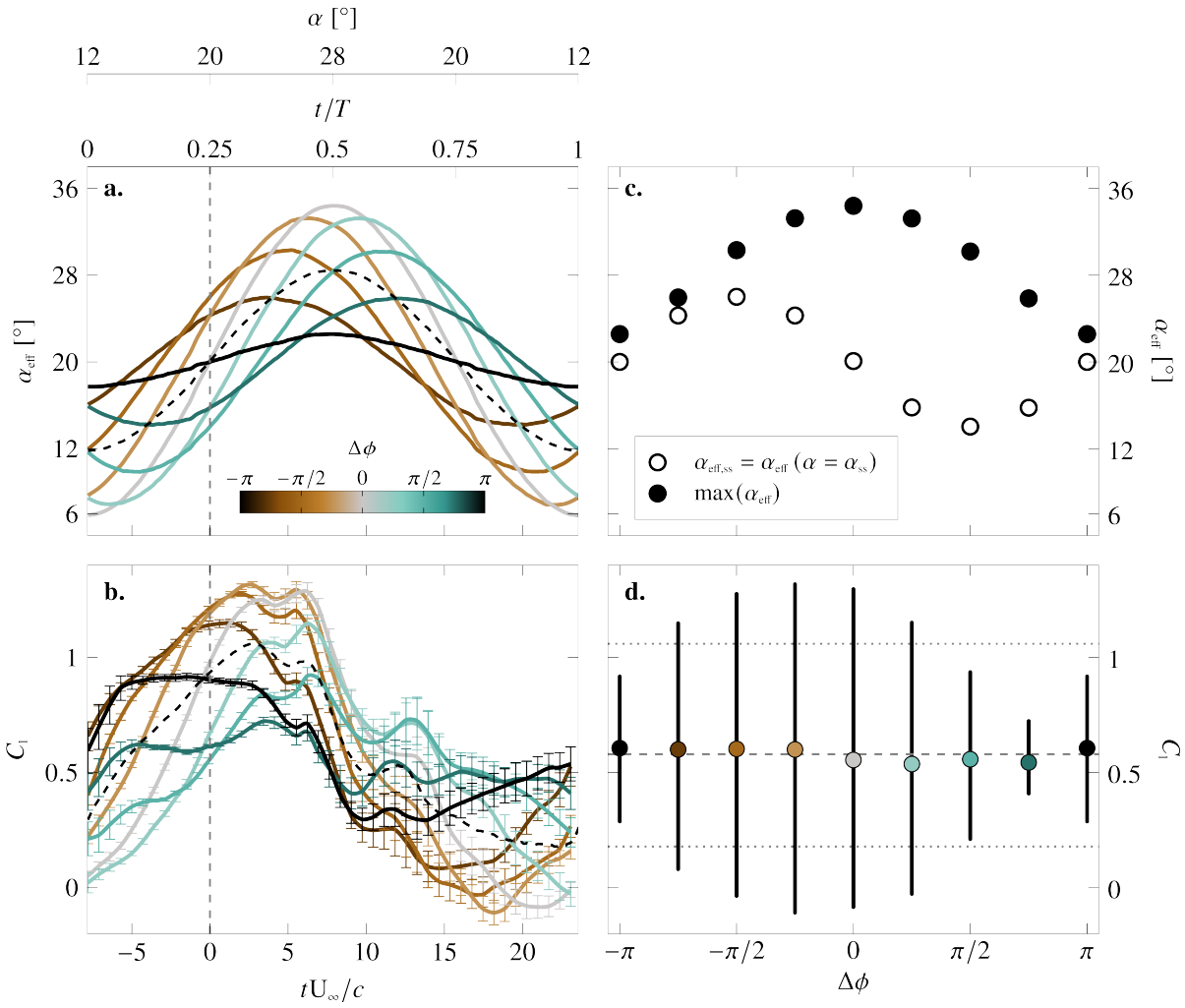

Figure 4 (a) Temporal evolution of the effective angle of attack, α_{eff} and (b) lift coefficient, C_l for different phase delays $\Delta\phi$ between the trailing-edge flap and the main wing oscillation. (c) The maximum effective angle and the effective angle at static stall for different phase delays and (d) time-average lift coefficient and C_l-range spanned for different phase delays. The dashed and dotted lines represents the time averaged lift coefficient and range for the motion with flap fixed at 0°.

to higher pre-stall lift values but also a more severe lift breakdown during stall and a larger range of C_l-values spanned within a pitching cycle. The lift response is influenced by the effective angle of attack amplitude as well as by the value of the effective angle of attack at pre-stall. The effective angle of attack amplitude is indicated by the maximum value of α_{eff}. The pre-stall values of the effective angle are represented by $\alpha_{eff,ss}$ which is the effective angle when the main airfoil is at the static stall angle α_{ss}.

C. Dynamic leading edge suction response for an oscillating trailing-edge flap

To assess the stall onset and investigate the influence of the flap motion on the stall delay, we analyse the evolution and critical values of the leading edge suction parameter (figure 5). The temporal evolution of the phase averaged

leading edge suction parameter A_0 is presented in figure 5b for different phase delays between the flap and the main wing. The leading edge suction parameter is more robust to oscillations of the trailing edge flap than the lift coefficient. The phase averaged evolution of the leading edge suction follow the same evolution for all oscillating flap motions as for the case with the flap fixed at 0° which is represented by the dashed line in figure 5b. In the beginning of the cycle, the leading edge suction increases approximately linearly until about 2 to 4 convective time units after the static stall angle is exceeded. Within the next 5 to 7 convective times, the values drop to a value of -0.13 and stay low for most of the second half of the cycle. Approximately 5 convective times before the end of the cycle, the leading edge suction starts to recover and increases to its initial values. The variations between the responses for different phase delays are much smaller than the variations within a pitching cycle. Nevertheless, we can identify the influence of the phase delay on the leading edge suction parameter (figure 5d). The triangular and circular symbols in figure 5d indicate respectively the maximum value of A_0 and its value at static stall. The dash-dotted lines represent the critical values of the static evolution of A_0 according to figure 3b and the dashed lines represent the critical values of the dynamic evolution of A_0 for same airfoil pitching motion with a fixed flap at $\beta = -20°$, 0°, and 20°.

The values of the leading edge suction at the static stall angle vary with the effective angle at static stall (open symbols in figure 3c-d). The maximum and minimum values of $A_{0,\mathrm{ss}}$ are found respectively for a phase delay of $-\pi/2$ and $\pi/2$ which corresponds to the motions with the highest and lowest effective angle of attack at the static stall angle. The values of $A_{0,\mathrm{ss}}$ for the in-phase and 180° out-of-phase motions are close to the static values for the fixed flap at 0°. In all of these three cases, the effective angle of attack equals the main wing angle of attack for $\alpha = 20°$. Prior to dynamic stall, the leading edge suction parameter is entirely driven by the instantaneous value of the effective angle of attack and is not influenced by the flap and wing dynamics nor the history effects of the motion.

The maximum values of the leading edge suction parameter and the corresponding effective angles of attack at which they occur are presented by the triangular symbols in figure 5c-d. The first important observation is the lack of a unique critical value of the leading edge suction. A flap deviation and a flap motion both affect the maximum values of the leading edge suction that can be obtained within a pitching cycle. The critical values for the various dynamic pitching oscillations are all higher than the maximum values for the static cases which are indicated by the dash-dotted lines in figure 5d. The overall highest and lowest maximum values are observed for a phase delay of $-\pi/4$ and $3\pi/4$, respectively. The values of $A_{0,\mathrm{max}}$ for these phase shifts are even higher, respectively lower, than the critical values measured for oscillations with a fixed flap angle of 20° and −20° which are indicated by the dashed lines in figure 5d. The higher values of $A_{0,\mathrm{max}}$ generally occur at higher effective angle of attacks. The correlation between the maximum leading edge suction and the effective angles of attack at static stall, at dynamic stall, and the maximum effective angle are summarised in figure 6. Here, we refer to dynamic stall as the moment at which the maximum leading edge suction parameter is reached which coincides with the start of the roll-up of the shear layer according to our previous work [25].

For a given absolute value of phase shift $|\Delta\phi|$ between the main wing and the flap oscillation, the same values of

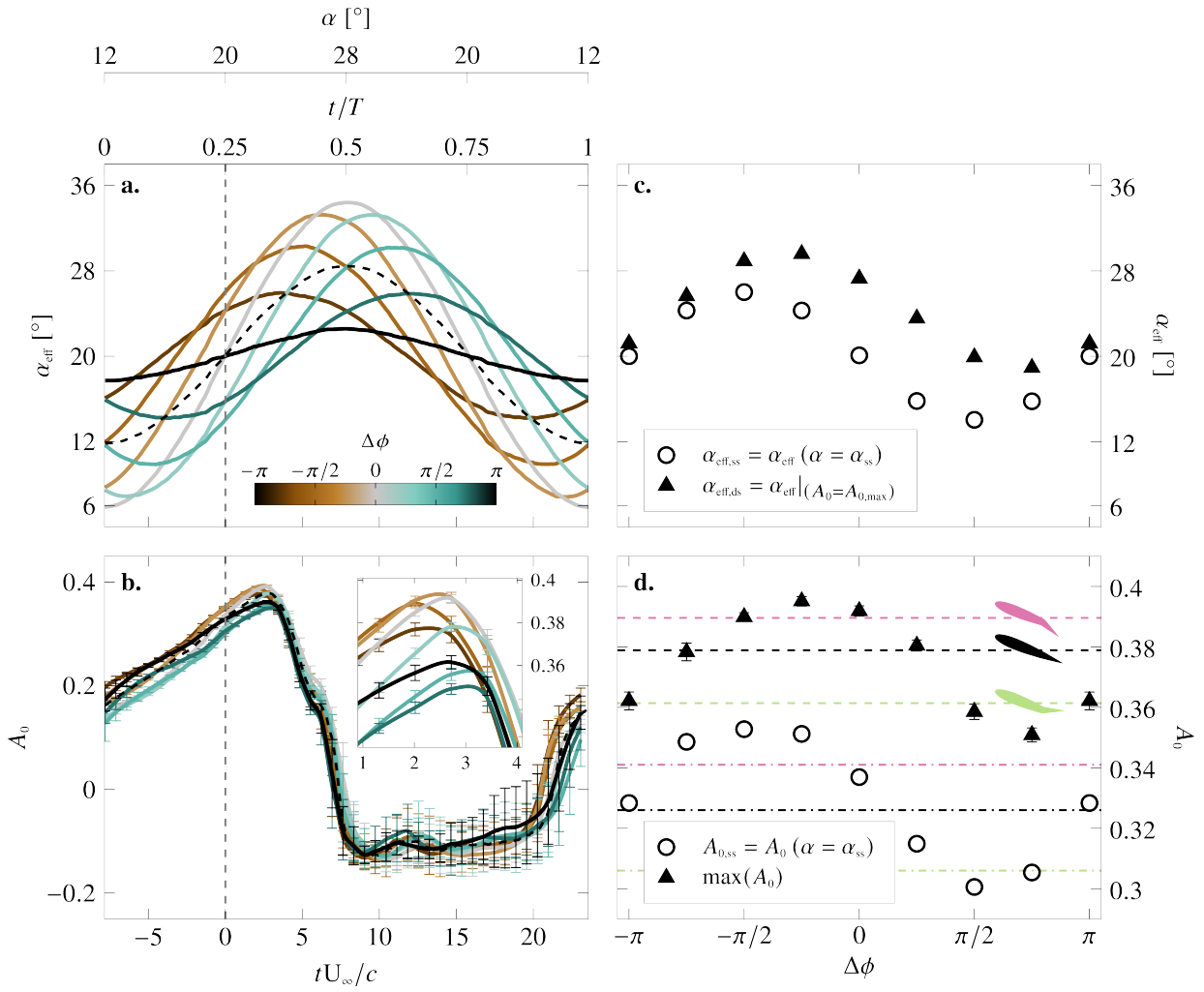

Figure 5 (a) Temporal evolution of the effective angle of attack, α_{eff} and (b) leading edge suction parameter, A_0 for different phase delays $\Delta\phi$ between the trailing-edge flap and the main wing oscillation. (c) The effective angle at static stall and dynamic stall for different phase delays and (d) A_0 at static and dynamic stall for different phase delays (d.). The dashed lines represent the maximum values of A_0 for a dynamically oscillating motion with flaps fixed at −20°, 0°, and 20°. The dash-dotted lines represent the maximum values of A_0 for a static response of the airfoil with flaps fixed at −20°, 0°, and 20°.

$\alpha_{eff,max}$ are obtained but the maximum values of A_0 are higher if the flap motion is leading ($\Delta\phi < 0$) than when the flap motion is lagging ($\Delta\phi > 0$) (figure 6a,c). The maximum effective angle and its value at static stall are not sufficient to predict the critical leading edge suction. In figure 6b, we do observe a linear relationship between $A_{0,max}$ and the corresponding effective angle of attack at the instant the leading edge suction parameter reaches it maximum value. Unless we know in advance at what angle dynamic stall occurs, this result does not allow us to predict the critical leading edge suction. It merely shows that dynamic stall occurs at higher effective angles of attack if the critical maximum value of the leading edge suction is higher. The question that remains is what causes the critical leading edge suction parameter to be increased for certain flap motions or what causes dynamic stall to be delayed to higher effective angles

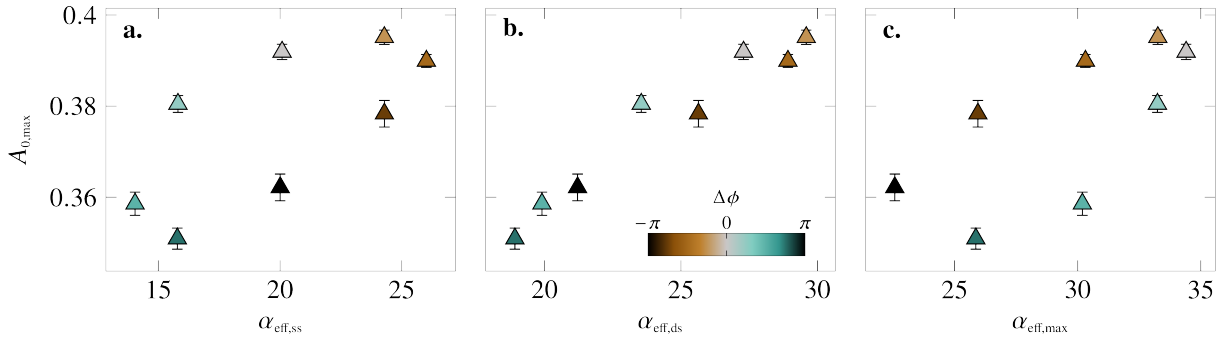

Figure 6 (a) Maximum value of the leading edge suction parameter versus effective angle of attack at static stall $\alpha_{\text{eff,ss}}$, (b) effective angle of attack at dynamic stall $\alpha_{\text{eff,ds}}$, and (c) the maximum value of the effective angle of attack $\alpha_{\text{eff,max}}$ for different phase shifts.

of attack in these cases. To answer these questions, we will focus next on the stall delay.

D. Variations of the dynamic stall delay

A dynamic stall delay $\Delta t \mathrm{U}_\infty / c$ is determined here as the convective time delay between the moment the main wing exceeds the static stall angle and moment $A_{0,\max}$ is reached. This corresponds to the duration of the primary stall development stage according to the nomenclature introduced in our previous work [25, 31]. During this first stage, the shear layer grows in wall-normal direction. It is followed by a second stage during which the shear layer rolls up and forms the primary stall vortex. The second stage ends with the separation of the primary stall vortex and its duration is related to a vortex formation time that is independent of the pitching motions kinematics.

The calculated values of the stall delay are presented in figure 7 versus phase shift, maximum value of the leading edge suction parameter, and and effective angle of attack at static stall, $\alpha_{\text{eff,ss}}$. The stall delay for a leading flap motion is generally lower than for a lagging flap motion and there is no injective functional relationship between the stall delay and the critical leading edge suction parameter (figure 7a,b). The stall delay is best described in terms of the effective angle of attack at static stall and decreases approximately linearly with increasing $\alpha_{\text{eff,ss}}$ (figure 7c). Higher values of $\alpha_{\text{eff,ss}}$ also lead to higher pre-stall lift values (figure 4c,d) and higher values of the leading edge suction parameter at static stall (figure 5c,d).

The above findings suggest that the effective angle at static stall is a measure for the vorticity generated at the airfoil's surface that will accumulate in the shear layer. Higher values of $\alpha_{\text{eff,ss}}$ yield stronger shear layers that will start to roll-up quicker resulting in a shorter stall delay. To corroborate this conclusion, we calculated the evolution of the leading edge circulation in the front 10 % of the airfoil. The results are summarized in figure 8. The integration area for the leading edge circulation Γ_{LE} is indicated in figure 8a by the coloured rectangle. The area covers the first 10 % of the airfoil's suction region starting from the leading edge stagnation point. The position of the leading edge stagnation point is determined as the extrapolated intersection of the stagnation line and the airfoil surface. The stagnation line is the ridge

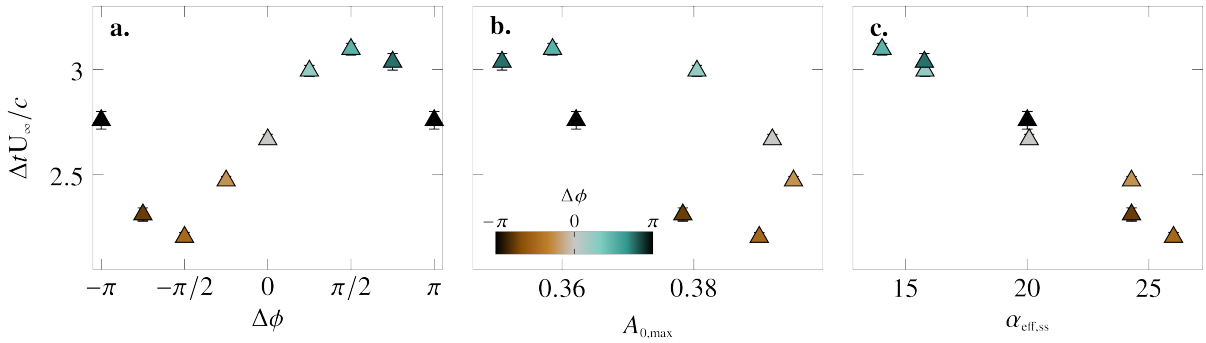

Figure 7 (a) Non-dimensional dynamic stall delay versus phase shift, (b) maximum value of the leading edge suction parameter, and (c) effective angle of attack at static stall.

of the positive finite-time Lyapunov exponent in the leading edge region. The circulation is calculated by integrating the tangential velocity along the edges of our rectangle. For different angles of attack, the size of the integration box is kept constant. The bottom of the box is aligned with the location of the leading edge stagnation point. The calculation is performed on the instantaneous PIV data and this information is then phase averaged. The resulting phase averaged circulation and its standard deviation are shown in figure 8b. The temporal evolution of the phase-averaged leading edge circulation values are presented in figure 8b for different phase shift of the flap motion. The dashed line indicates the results of the oscillation with fixed flap at 0°. The flap motions have a measurable influence on the leading edge circulation but the general evolution is similar for all flap motions. The circulation increases in the first part of the cycle and reaches a maximum value shortly after $A_{0,\max}$ is reached which is indicated by the gray shaded region. Thereafter, the circulation drops rapidly for all cases down to the same value of approximately 1.2.

Characteristic values of leading edge circulation at static and dynamic stall are presented in figure 8c versus phase shift and in figure 8d versus the corresponding effective angles of attack when the values are extracted. The leading edge circulation values at static and dynamic stall are higher when the flap motion leads than when the flap motion lags. More generally, the leading edge circulation increases approximately linearly with increasing effective angle of attack for the values extracted at static and dynamic stall. This confirms our previous conclusion that a higher effective angle at static stall results in higher leading edge circulation, which then leads to a higher leading edge suction parameter and lift. The stronger shear layer also promotes the rolling-up of the shear layer and results in a shorter stall delay.

E. Thin-airfoil theory based model

The experimental results for the leading edge suction parameter suggest that the A_0 is primarily driven by the instantaneous values of the effective angle of attack. If this is indeed the case, we should be able to predict the influence of a trailing-edge flap motion based on thin-airfoil theory. According to thin-airfoil theory, the influence of a trailing-edge flap on the leading edge suction parameter can be estimated by a superposition of the solution for the

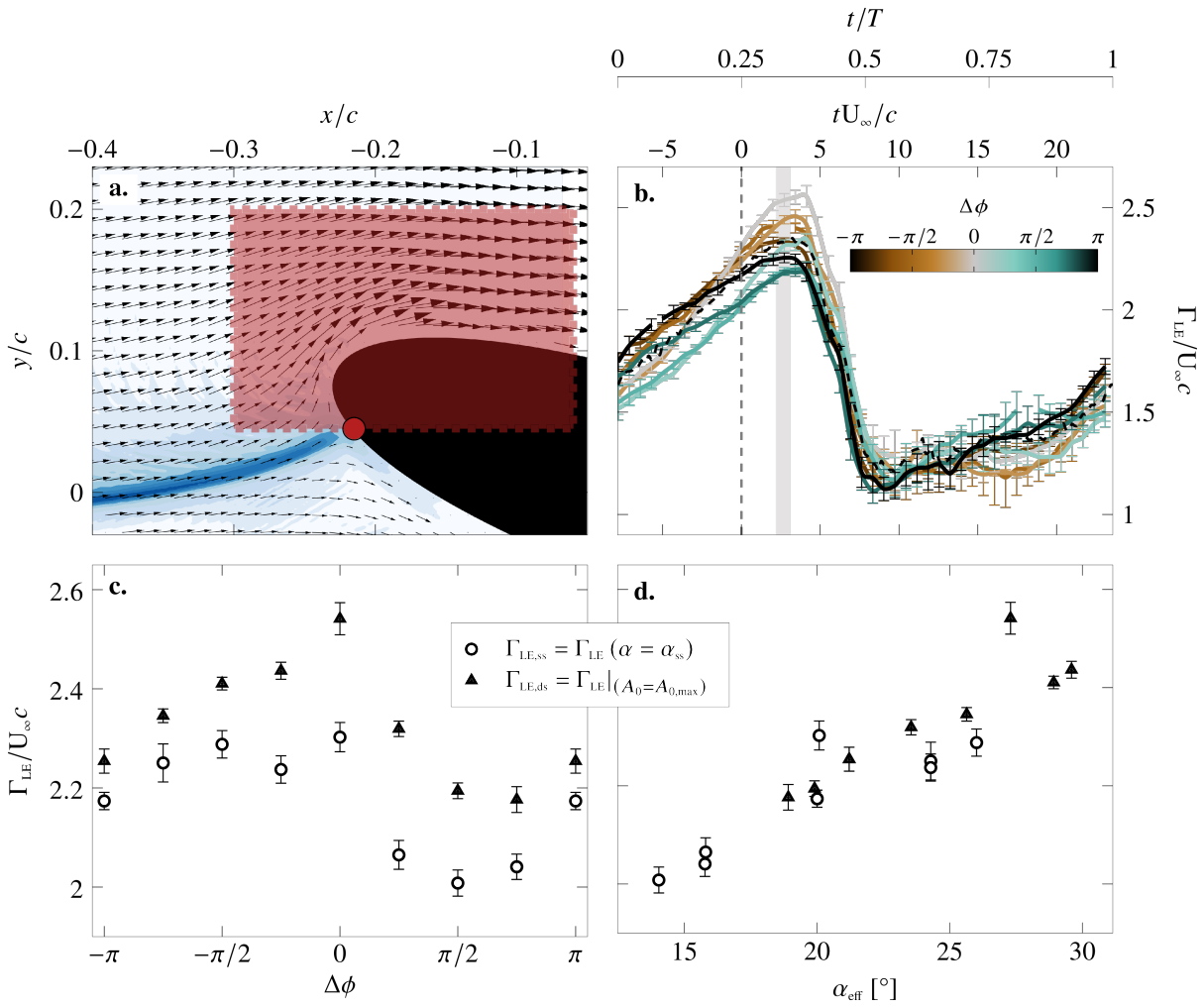

Figure 8 (a) Integration region for the leading edge circulation, (b) temporal evolution of the leading edge circulation, variation of leading edge circulation values at static, (c) dynamic stall versus phase shift between the flap and the main wing oscillation and (d) dynamic stall versus the corresponding effective angle of attack.)

airfoil without flap and the solution for the isolated flap $A_0 = A_{0,\mathrm{noflap}} + A_{0,\mathrm{flap}}$ [32]. The solution for the flap is given by:

$$A_{0,\mathrm{flap}} = K_\mathrm{f} \tan\beta \tag{4}$$

with β the flap angle and

$$K_\mathrm{f} = 1 - \Phi/\pi\,, \tag{5}$$

where Φ is the chord-normalised hinge position of the trailing-edge flap of length l_{flap} defined such that:

$$1 - l_{\mathrm{flap}} = \frac{1}{2}(1 - \cos\Phi)\,. \tag{6}$$

For the given geometry with $l_{flap} = 0.3$, we obtain $K_f = 0.37$.

We can also estimate the coefficient K_f from the static experimental results of the leading edge suction parameter as a function of angle of attack (figure 3b). The vertical shift of the static curves for the fixed flap angles $\beta \in \{-20°, -10°, 10°, 20°\}$ with respect to the results for the case with $\beta = 0°$ should be equal to $K_f \tan\beta$. By linearly fitting the pre-stall static A_0 versus α for the different fixed β values we obtain an experimental coefficient $K_{f,exp} = 0.053$ which is an order of magnitude lower than the coefficient calculated directly from the geometric parameters $K_{f,geo} = 0.37$. The difference is attributed to the influence of the open jet test section and relative thickness of our airfoil.

We now use the flap coefficient $K_{f,exp} = 0.053$ to obtain a first order estimate of the influence of the flap motion on the leading edge suction parameter by adding the contribution $K_{f,exp} \tan\beta$ to the experimental results for the pitching motion with fixed flap at 0°. The results of thin-airfoil theory based estimates and their deviation with respect to the experimental results are presented in figure 9a and b. We focus here only on the stall development part of the cycle. In general, the deviations between the experimental and theoretical results are less than 5 % of the maximum A_0 value during pre-stall. The thin-airfoil model tends to underestimate the leading edge suction parameter when the flap motion is leading and overestimate when the flap motion is lagging with respect to the main wing motion. The error is lower for the leading flap motion. The estimated values at static stall and the maximum values of A_0 are well predicted by the thin-airfoil model and correctly reflect the influence of the flap motion (figure 9c). The timing of the maximum leading edge suction, what we referred to as the stall delay, is not captured by the model. The timing based on the thin-airfoil model fluctuates around the experimental values found for the in-phase and 180° out-of-phase motions. The experimentally observed variations for the other phase shifts are not captured by the theoretical model. The thin-airfoil theory based model only takes into account the instantaneous flap angles and does not consider any influence of the pitch rate nor the history of the flap motion. The value of the leading edge suction is primarily driven by the instantaneous effective angle of attack (figure 6b) and can be predicted by the thin-airfoil approach suggested here. The dynamic stall delay is strongly influenced by the pre-stall evolution of the effective angle of attack and not just the instantaneous values (figure 7c) and can not be predicted by this simple model. These results further support the idea that dynamic stall development is governed by critical stall delays rather than a critical maximum leading edge suction parameter.

IV. Conclusions

The flow around a pitching NACA0015 airfoil with an oscillating trailing-edge flap is investigated using two-dimensional time-resolved particle image velocimetry and surface pressure measurements. The airfoil pitches around its static stall angle of attack and the flap either oscillates with the same frequency as the main wing around its neutral position or is fixed at a constant deflection angle. The phase shift between the oscillation of the flap and the main wing is varied to create different temporal evolutions of the geometric effective angle of attack. The objective of the study is to characterise the influence of the trailing-edge flap kinematics on the development of dynamic stall. We specifically focus

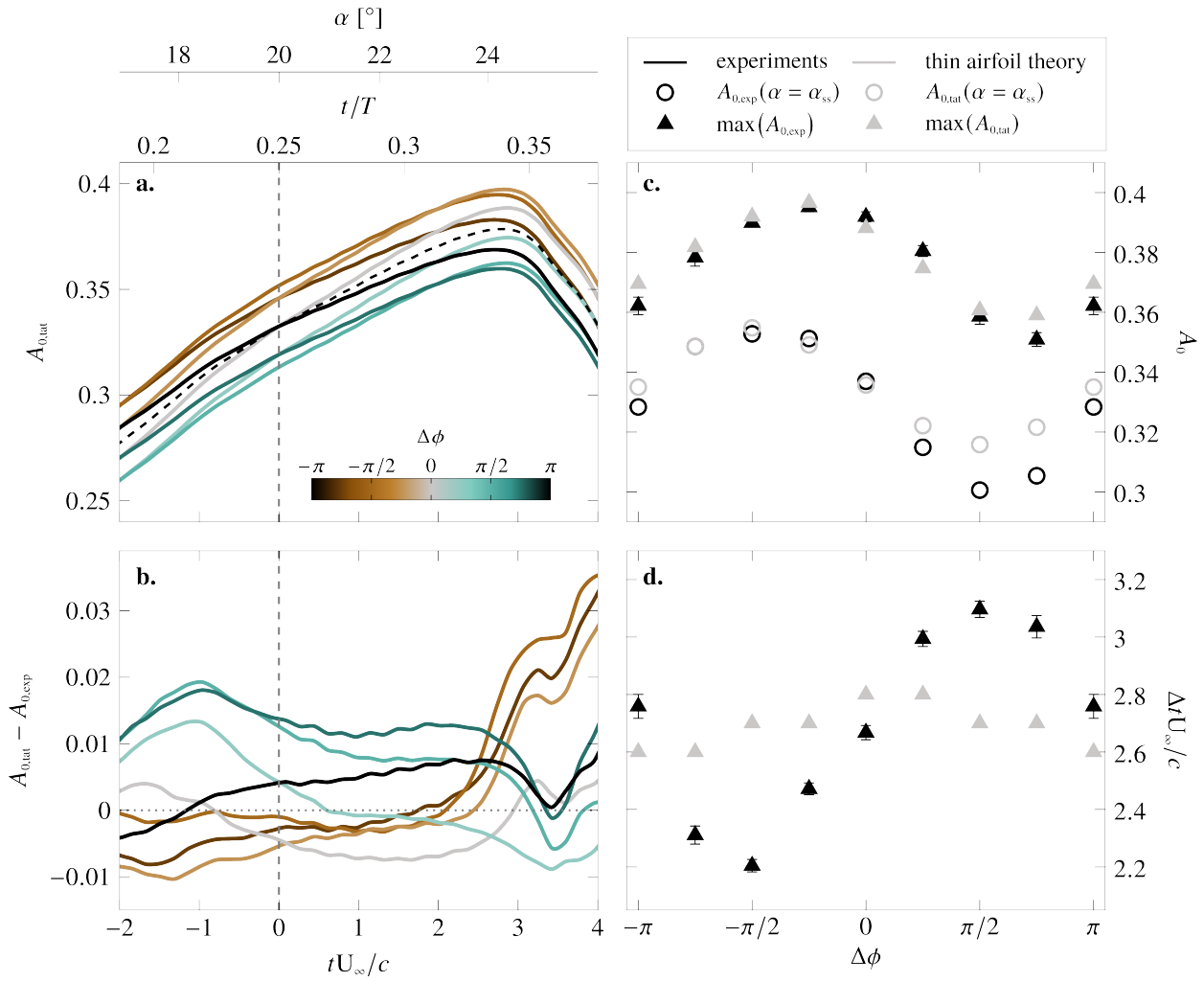

Figure 9 (a) Evolution of the leading edge suction parameter based on thin-airfoil theory, (b) deviation between of the model estimate and the experimental values, (c) comparison of the experimental and theoretical values of A_0 at static stall and the maximum values (c.), and (d) comparison of timing of the experimental and theoretical maximum A_0.

on the timing of the stall development and on the critical values of the leading edge suction parameter as a potential stall trigger.

A static or dynamic trailing-edge flap motion significantly affects the static and dynamic stall lift response but preserves the characteristic evolution of the leading edge suction parameter. Subtle variations of the magnitude of the leading edge suction are linearly related to the static flap defection angles or the instantaneous effective angle of attack at static or dynamic stall. Higher effective angles lead to higher values of the leading edge suction parameter. A thin-airfoil theory based model that linearly superimposes the effect of the flap on the response for a fixed flap in its neutral position correctly predicts the maximum values of the leading edge suction parameter.

The moment in time at which the maximum leading edge suction parameter is reached coincides with the start of the

roll-up of the shear layer and is considered to mark dynamic stall onset here. Its time delay with respect to the moment at which the static stall angle is exceeded is referred to as the dynamic stall delay. The stall delay is not determined solely by the instantaneous effective angle but is influenced by the flap dynamics and the pre-stall temporal evolution of the effective angle of attack. For the trailing-edge flap oscillations considered here, the stall delay is best described in terms of the effective angle of attack at static stall and decreases linearly with increasing $\alpha_{\text{eff,ss}}$. The decrease in the stall delay is due to an increase in the production of vorticity at the airfoil's surface for higher pre-stall effective angles of attack. This leads to a stronger shear layer that will start to roll-up quicker resulting in a shorter stall delay. The maximum leading edge suction value at dynamic stall is given by the instantaneous effective angle at the end of the stall delay. Dynamic stall development is thus governed by critical stall delays rather than a critical maximum leading edge suction parameter.

Acknowledgments

We thank Sabrina Henne and the DLR staff for their assistance and support during the measurement campaign and the EPFL mechanics workshop, in particular Marc Jeanneret, for their invaluable support and advice for the design and construction of the pitching airfoil test rig.

The work presented is supported by the SNSF Lead Agency programme under grant number 200021E-169841 and by the SNSF Assistant Professor energy grant number PYAPP2_173652.

References

[1] Carr, L. W., "Progress in analysis and prediction of dynamic stall," *Journal of Aircraft*, Vol. 25, No. 1, 1988, pp. 6–17. doi:10.2514/3.45534.

[2] Alrefai, M., and Acharya, M., "Controlled leading-edge suction for management of unsteady separation over pitching airfoils," *AIAA Journal*, Vol. 34, No. 11, 1996, pp. 2327–2336. doi:10.2514/3.13398.

[3] Karim, M. A., and Acharya, M., "Suppression of dynamic-stall vortices over pitching airfoils by leading-edge suction," *AIAA Journal*, Vol. 32, No. 8, 1994, pp. 1647–1655. doi:10.2514/3.12155.

[4] Fukumoto, H., Aono, H., Watanabe, T., Tanaka, M., Matsuda, H., Osako, T., Nonomura, T., Oyama, A., and Fujii, K., "Control of dynamic flowfield around a pitching NACA633-618 airfoil by a DBD plasma actuator," *International Journal of Heat and Fluid Flow*, Vol. 62, 2016, pp. 10–23. doi:10.1016/j.ijheatfluidflow.2016.10.012.

[5] Iwasaki, Y., Nonomura, T., Nankai, K., Asai, K., Kanno, S., Suzuki, K., Komuro, A., Ando, A., Takashima, K., Kaneko, T., Yasuda, H., Hayama, K., Tsujiuchi, T., Nakajima, T., and Nakakita, K., "Dynamic Stall Control around Practical Airfoil Using Nanosecond-Pulse-Driven Dielectric Barrier Discharge Plasma Actuators," *Energies*, Vol. 13, No. 6, 2020, p. 1376. doi:10.3390/en13061376, URL `https://www.mdpi.com/1996-1073/13/6/1376`.

[6] Singhal, A., Castañeda, D., Webb, N., and Samimy, M., "Control of Dynamic Stall over a NACA 0015 Airfoil Using Plasma

Actuators," *AIAA Journal*, Vol. 56, No. 1, 2018, pp. 78–89. doi:10.2514/1.J056071, URL https://arc.aiaa.org/doi/10.2514/1.J056071.

[7] Yu, Y. H., Lee, S., McAlister, K. W., Tung, C., and Wang, C. M., "Dynamic stall control for advanced rotorcraft application," *AIAA Journal*, Vol. 33, No. 2, 1995, pp. 289–295. doi:10.2514/3.12496.

[8] Chandrasekhara, M. S., Wilder, M. C., and Carr, L. W., "Unsteady stall control using dynamically deforming airfoils," *AIAA Journal*, Vol. 36, No. 10, 1998, pp. 1792–1800. doi:10.2514/2.294.

[9] Kim, J. S., Smith, E. C., and Wang, K. W., "Active load control of an articulated composite rotor blade via dual trailing edge flaps," *Collection of Technical Papers - AIAA/ASME/ASCE/AHS/ASC Structures, Structural Dynamics and Materials Conference*, Vol. 2, 2003, pp. 1329–1340. doi:10.2514/6.2003-1543.

[10] Feszty, D., Gillies, E. A., and Vezza, M., "Alleviation of airfoil dynamic stall moments via trailing-edge-flap flow control," *AIAA Journal*, Vol. 42, No. 1, 2004, pp. 17–25. doi:10.2514/1.853.

[11] Gerontakos, P., and Lee, T., "Trailing-edge flap control of dynamic pitching moment," *AIAA Journal*, Vol. 45, No. 7, 2007, pp. 1688–1694. doi:10.2514/1.27577.

[12] Rennie, R. M., and Jumper, E. J., "Experimental measurements of dynamic control surface effectiveness," *Journal of Aircraft*, Vol. 33, No. 5, 1996, pp. 880–887. doi:10.2514/3.47030.

[13] Medina, A., Ol, M. V., Mancini, P., and Jones, A., "Revisiting Conventional Flaps at High Deflection Rate," *AIAA Journal*, Vol. 55, No. 8, 2017, pp. 2676–2685. doi:10.2514/1.J055754, URL https://arc.aiaa.org/doi/10.2514/1.J055754.

[14] Medina, A., Hemati, M. S., and Rockwood, M., "Separated Flow Response to Rapid Flap Deflection," *AIAA Journal*, 2020, pp. 1–12. doi:10.2514/1.J058367, URL https://arc.aiaa.org/doi/10.2514/1.J058367.

[15] Pohl, J., Semaan, R., and Jones, A. R., "Dynamic lift measurements on an airfoil with periodic flap motion at high reynolds number," *AIAA Scitech 2019 Forum*, American Institute of Aeronautics and Astronautics Inc, AIAA, 2019. doi:10.2514/6.2019-1396.

[16] Gerontakos, P., and Lee, T., "Dynamic stall flow control via a trailing-edge flap," *AIAA Journal*, Vol. 44, 2006, pp. 469–480. doi:10.2514/1.17263.

[17] Shen, J., Yang, M., and Chopra, I., "Swashplateless helicopter rotor with trailing-edge flaps for flight and vibration control," *Journal of Aircraft*, Vol. 43, No. 2, 2006, pp. 346–352. doi:10.2514/1.14634.

[18] Krzysiak, A., and Narkiewicz, J., "Aerodynamic loads on airfoil with trailing-edge flap pitching with different frequencies," , mar 2006. doi:10.2514/1.15597.

[19] Lee, T., and Su, Y. Y., "Unsteady airfoil with a harmonically deflected trailing-edge flap," *Journal of Fluids and Structures*, Vol. 27, No. 8, 2011, pp. 1411–1424. doi:10.1016/j.jfluidstructs.2011.06.008.

[20] Ramesh, K., Gopalarathnam, A., Edwards, J. R., Ol, M. V., and Granlund, K., "An unsteady airfoil theory applied to pitching motions validated against experiment and computation," *Theoretical and Computational Fluid Dynamics*, Vol. 27, No. 6, 2013, pp. 843–864. doi:10.1007/s00162-012-0292-8.

[21] Ramesh, K., Gopalarathnam, A., Granlund, K., Ol, M. V., and Edwards, J. R., "Discrete-vortex method with novel shedding criterion for unsteady aerofoil flows with intermittent leading-edge vortex shedding," *Journal of Fluid Mechanics*, Vol. 751, 2014, pp. 500–538. doi:10.1017/jfm.2014.297.

[22] Ramesh, K., Granlund, K. O., Ol, M. V., Gopalarathnam, A., and Edwards, J. R., "Leading-edge flow criticality as a governing factor in leading-edge vortex initiation in unsteady airfoil flows," *Theoretical and Computational Fluid Dynamics*, Vol. 32, No. 2, 2017, p. 109 136. doi:10.1007/s00162-017-0442-0, URL https://link.springer.com/article/10.1007/s00162-017-0442-0.

[23] Saini, A., and Gopalarathnam, A., "Leading-Edge Flow Sensing for Aerodynamic Parameter Estimation," *AIAA Journal*, Vol. 56, No. 12, 2018. doi:10.2514/1.J057327.

[24] Hou, W., Darakananda, D., and Eldredge, J. D., "Machine-Learning-Based Detection of Aerodynamic Disturbances Using Surface Pressure Measurements," *AIAA Journal*, 2019, p. 1–15. doi:10.2514/1.j058486.

[25] Deparday, J., and Mulleners, K., "Modeling the interplay between the shear layer and leading edge suction during dynamic stall," *Physics of Fluids*, Vol. 31, No. 10, 2019, p. 107104. doi:10.1063/1.5121312.

[26] Ewald, B., "Wind tunnel wall corrections," Agard-ag-336, 1998.

[27] Evans, W. T., and Mort, K. W., *Analysis of computed flow parameters for a set of sudden stalls in low-speed two-dimensional flow*, D-85, 1959.

[28] James, E. C., "Leading Edge Separation Criterion for an Oscillating Airfoil," *Workshop on Unsteady separated flow*, 1983. doi:10.21236/adp004175.

[29] Harms, T., Nikoueeyan, P., and Naughton, J. W., "An Experimental Evaluation of Cycle-to-Cycle Variations of Dynamic Stall," 2018. doi:10.2514/6.2018-1267.

[30] Smith, M. J., Jones, A. R., Ayancik, F., Mulleners, K., and Naughton, J. W., "An Assessment of the State-of-the-Art from the 2019 ARO Dynamic Stall Workshop," 2020. doi:10.2514/6.2020-2697.

[31] Mulleners, K., and Raffel, M., "Dynamic stall development," *Experiments in Fluids*, Vol. 54, No. 2, 2013, pp. 1469–1477. doi:10.1007/s00348-013-1469-7.

[32] Houghton, E., Carpenter, P., Collicott, S. H., and Valentine, D. T., "Chapter 6 - Thin Airfoil Theory," *Aerodynamics for Engineering Students (Seventh Edition)*, edited by E. Houghton, P. Carpenter, S. H. Collicott, and D. T. Valentine, Butterworth-Heinemann, 2017, seventh edition ed., pp. 391 – 447. doi:https://doi.org/10.1016/B978-0-08-100194-3.00006-7, URL http://www.sciencedirect.com/science/article/pii/B9780081001943000067.